Polymer 51 (2010) 5576–5584

Contents lists available at ScienceDirect

Polymer

journal homepage: www.elsevier.com/locate/polymer

Crystal orientation of poly(ε-caprolactone) blocks confined in crystallized polyethylene lamellar morphology of poly(ε-caprolactone)-*block*-polyethylene copolymers

Tomoki Higa, Hikaru Nagakura, Takuya Sakurai, Shuichi Nojima*

Department of Organic and Polymeric Materials, Graduate School of Science and Engineering, Tokyo Institute of Technology, H-125, 2-12-1 Ookayama Meguro-Ku, Tokyo 152-8552, Japan

ARTICLE INFO

Article history:
Received 8 May 2010
Received in revised form
25 August 2010
Accepted 15 September 2010
Available online 8 October 2010

Keywords:
Crystalline–crystalline diblock copolymer
Spatial confinement
Crystal orientation

ABSTRACT

The crystal orientation of poly(ε-caprolactone) (PCL) blocks in PCL-*block*-polyethylene (PE) copolymers has been investigated using two-dimensional small-angle X-ray scattering (2D-SAXS) and 2D wide-angle X-ray diffraction (2D-WAXD) as a function of crystallization temperature T_c and thickness of PCL layers d_{PCL}. The PCL blocks were spatially confined in the solid lamellar morphology formed by the crystallization of PE blocks (PE lamellar morphology), an alternating structure of crystallized PE lamellae and amorphous PCL layers. This confinement is expected to be intermediate between hard confinement by glassy lamellar microdomains and soft confinement by rubbery ones, because the crystallized PE lamellae consist of hard PE crystals covered with amorphous (or soft) PE blocks. The 2D-SAXS results showed uniaxial orientation of the PE lamellar morphology after applying the rotational shear to the sample. Therefore, it was possible to investigate crystal orientation of PCL blocks within the oriented PE lamellar morphology. The 2D-WAXD results revealed that the *c* axis of PCL crystals (i.e., stem direction of PCL chains) was parallel to the lamellar surface normal irrespective of T_c when 16.5 nm $\geq d_{PCL} \geq$ 10.7 nm. However, it changed significantly with changing T_c when $d_{PCL} = 8.8$ nm; the *c* axis was perpendicular to the lamellar surface normal at 45 °C $\geq T_c \geq$ 25 °C while it was almost random at 20 °C $\geq T_c \geq$ 0 °C. These results suggest that the PE lamellar morphology plays a similar role to glassy lamellar microdomains regarding spatial confinement against subsequent PCL crystallization.

1. Introduction

Morphology formation occurring in crystalline–amorphous diblock copolymers is extremely complicated due to the interplay between microphase separation and crystallization. Many research groups have reported such morphology formation as a function of molecular characteristics of constituent copolymers [1–4]. For example, it is well known that when the glass transition temperature of amorphous blocks T_g is sufficiently higher than the crystallization temperature of crystalline blocks T_c or two blocks are strongly segregated to form a stable microdomain structure, crystallization occurs within this structure to yield the crystallized microdomain structure (i.e., confined crystallization) [5–15].

In confined crystallization, the relationship between anisotropy of existing cylindrical or lamellar microdomains and orientation of lamellar crystals formed in it is an interesting research subject. For example, the crystallization behavior and crystal orientation of block chains confined in the glassy lamellar morphology (i.e., $T_g > T_c$) have been extensively investigated as a function of T_c and confinement size *d* between glassy layers [16–23]. It is known that the *c* axis of lamellar crystals (i.e., stem direction of folded chains) is parallel to the lamellar surface normal when *d* is larger than the critical value d^* while it is perpendicular when $d < d^*$ and finally it is random at extremely small *d*. It is also reported that the crystallization temperature significantly affects the orientation degree of lamellar crystals formed between glassy layers. Thus, the crystal orientation depends significantly on *d* and T_c when crystalline blocks are completely confined in the glassy lamellar microdomains.

Ho et al. [24] have investigated the crystal orientation of block chains confined in the rubbery and glassy lamellar microdomains using strongly segregated poly(L-lactide)-*block*-polystyrene (PLLA-*b*-PS) copolymers. They found that completely confined crystallization mentioned above was observed when $T_g > T_c$ (*hard confinement*). However, crystallization made the lamellar morphology undulated when $T_g < T_c$ (*soft confinement*), but the *c* axis of existing crystals was always parallel to the lamellar surface normal. They

* Corresponding author. Tel.: +81 3 5734 2132; fax: +81 3 5734 2888.
E-mail address: snojima@polymer.titech.ac.jp (S. Nojima).

0032-3861/$ – see front matter © 2010 Elsevier Ltd. All rights reserved.
doi:10.1016/j.polymer.2010.09.039

interpreted that the undulated lamellar morphology was allowed by the rubbery nature of confined materials in order to increase the total crystallinity of PLLA blocks.

We have recently investigated the crystallization behavior and resulting morphology of a crystalline–crystalline diblock copolymer, poly(ε-caprolactone)-*block*-polyethylene (PCL-*b*-PE) [25–29], where the crystallizable temperature of PCL blocks was sufficiently lower than that of PE blocks. Therefore, when PCL-*b*-PE was quenched from the microphase-separated melt into low temperatures, the PE blocks crystallized first to form the solid lamellar morphology, an alternating structure consisting of crystallized PE lamellae and amorphous PCL layers (PE lamellar morphology), followed by the crystallization of PCL blocks starting from this morphology. In such a case, the PE lamellar morphology will be a kind of spatial confinement against the subsequent crystallization of PCL blocks. This confinement is expected to be intermediate between hard confinement by glassy lamellar microdomains and soft confinement by rubbery ones, because the crystallized PE lamellae consist of hard PE crystals covered with amorphous (or soft) PE blocks. In this study, we investigate the crystal orientation of PCL blocks spatially confined in the PE lamellar morphology formed in PCL-*b*-PE as a function of T_c and confinement size (i.e., thickness of PCL layers) d_{PCL}. We clarify how the PE lamellar morphology affects the crystal orientation of PCL blocks by comparing our results with those for hard (or glassy) and soft (or rubbery) confinements.

2. Experimental

2.1. Samples

The block copolymers used in this study are poly(ε-caprolactone)-*block*-polyethylene (PCL-*b*-PE) with various compositions, which were obtained by the hydrogenation of PCL-*block*-polybutadiene (PCL-*b*-PB) diblocks anionically synthesized. The methods of PCL-*b*-PB synthesis and hydrogenation of PB blocks were described elsewhere [25,26]. The results of molecular characterization are shown in Table 1, where the melting temperature (and also crystallizable temperature) of PE blocks $T_{m,PE}$ (~100 °C) is sufficiently higher than that of PCL blocks $T_{m,PCL}$ (~55 °C), so that the PE blocks crystallize first followed by the crystallization of PCL blocks when PCL-*b*-PE is quenched from the microphase-separated melt into low temperatures. It is found from our previous studies [25–27] that the crystallization of PE blocks destroys the molten microdomain structure to form the solid lamellar morphology consisting of crystallized PE lamellae and amorphous PCL layers. Following specific volumes were used to calculate the volume fraction of each block in PCL-*b*-PE. For amorphous PE [30],

$$v_{sp}(T) = 1.1696 + \left(1.77 \times 10^{-4}\right) \times T \quad (1)$$

and for amorphous PCL [31].

$$v_{sp}(T) = 0.9106 + \left(6.01 \times 10^{-4}\right) \times T \quad (2)$$

where $v_{sp}(T)$ is in cm^3/g and T in °C.

2.2. Differential scanning calorimetry (DSC) measurements

DSC measurements were performed using Perkin Elmer DSC Pyris 1 during cooling from the microphase-separated melt at −5 °C/min to obtain the crystallizable temperatures of each block, $T_{c,PE}$ and $T_{c,PCL}$, and also during heating at 5 °C/min to obtain $T_{m,PE}$ and $T_{m,PCL}$. The samples were isothermally crystallized at 0 °C for 5 min before heating. The crystallinity of each block was evaluated from the endothermic area of the DSC thermogram during heating assuming that the heat of fusion for perfect PCL and PE crystals was 135 J/g [30] and 277 J/g [31], respectively.

2.3. Orientation of PE lamellar morphology

A disk sample with the diameter of *ca.* 10 mm and the thickness of *ca.* 1.0 mm was subject to the rotational shear at 80 °C (where PE blocks crystallized and PCL blocks amorphous) for 3 h under a dry nitrogen atmosphere using Linkam shearing cell (CSS-450) to uniaxially orient the PE lamellar morphology [32]. The angular velocity applied was 6.28 rad/s, which corresponded to the shear rate of 70 s^{-1}. After cooling the sample into room temperature, a small amount of specimen was cut out from the disk for crystallization experiments.

2.4. One-dimensional small-angle X-ray scattering (1D-SAXS) measurements

The microdomain structure of the molten PCL-*b*-PE and the unoriented lamellar morphology formed after crystallization of PE blocks were first investigated using synchrotron small-angle X-ray scattering (SR-SAXS), which was performed at Photon Factory in High Energy Accelerator Research Organization, Tsukuba Japan, with a small-angle X-ray equipment for solution (SAXES) installed at beam-line BL-10C. Details of the equipment and the instrumentation are described in our publications [28,33]. The scattered intensity was recorded with a one-dimensional position-sensitive proportional counter, by which isotropic scattering was obtained as a function of wave number s ($= (2/\lambda)\sin\theta$, λ: X-ray wavelength (=0.1488 nm) and 2θ: scattering angle). The long period, an alternating distance of the lamellar morphology or microdomain structure, was evaluated from the angular position of the primary intensity peak to confirm the morphological transition from the microdomain structure into the solid lamellar morphology by the crystallization of PE blocks.

2.5. Two-dimensional SAXS (2D-SAXS) and 2D wide-angle X-ray diffraction (2D-WAXD) measurements

Simultaneous 2D-SAXS and 2D-WAXD measurements were performed using a Rigaku Nano-Viewer with a rotating-anode

Table 1
Molecular characteristics of PCL-*b*-PE used in this study.

Sample Code	Total M_n[a]	M_w/M_n[a]	PCL:PE[b] (vol.%)	$T_{m,PCL}$[c] (°C)	$T_{m,PE}$[c] (°C)	χ_{PE}[c] (%)	L[d] (nm)	d_{PCL}[e] (nm)
CL11	23,400	1.03	11:89	–	98	–	–	–
CL33	13,700	1.05	33:67	53	98	21.0	25.0	8.8
CL38	13,800	1.12	38:62	54	101	23.5	26.6	10.7
CL46	9700	1.14	46:54	55	100	29.4	24.2	11.7
CL51	27,800	1.07	51:49	57	100	20.9	31.7	16.5

[a] Determined by GPC with polystyrene as a standard.
[b] Determined by ^{1}H-NMR.
[c] Determined by DSC during heating at 5 °C/min.
[d] Long period evaluated from 1D-SAXS.
[e] Thickness of PCL layers calculated from L and the volume fraction of PE and PCL blocks by considering the crystallinity of PE blocks.

X-ray generator operating at 45 kV and 60 mA. The wavelength used was 0.1542 nm of CuKα radiation. The detector was an image plate (FUJI Film BAS-SR 127) with the size of 10 × 10 cm^2, and the accumulation time was 1 h. The WAXD intensity at selected diffraction angles was plotted against azimuthal angle ϕ after subtracting the background scattering to decide the orientation of PCL crystals confined in the PE lamellar morphology and also to evaluate the degree of PCL crystal orientation *f*. The method to evaluate *f* is described in Section 3.3.

3. Results and discussion

3.1. Characterization of PCL-b-PE copolymers and orientation of PE lamellar morphology

Fig. 1 shows the DSC thermogram of CL51 during cooling at −5 °C/min from 120 °C (microphase-separated melt) into 0 °C and during heating at 5 °C/min from 0 °C into 120 °C. We find two exothermic peaks at *ca.* 85 °C and 35 °C during cooling, which correspond to the crystallization of PE and PCL blocks, respectively. It is obvious from Fig. 1 that the PE block crystallizes first followed by the crystallization of PCL blocks, which starts from the morphology just formed by the crystallization of PE blocks. We also find two endothermic peaks at *ca.* 57 °C and 100 °C during heating, indicating independent melting of PCL and PE blocks. These DSC curves were obtained for every PCL-*b*-PE except for CL11, where the exothermic peak of PCL blocks during cooling, as well as the endothermic peak during heating, was too faint because of the extremely small amount of PCL blocks. Therefore, reliable values could not be obtained for CL11. We find from Fig. 1 that it is possible to repeatedly crystallize and melt PCL blocks in CL33–CL51 within the solid morphology formed by the crystallization of PE blocks as far as the sample is treated at $T < T_{m,PE}$.

Fig. 2 shows the 1D-SAXS curves of CL46 measured at 120 °C (microphase-separated), 70 °C (PE blocks crystallized and PCL blocks amorphous), and 25 °C (both blocks crystallized). The SAXS curve at 120 °C has a couple of sharp scattering peaks, the angular positions of which exactly correspond to a ratio of 1:2:3, indicating that the lamellar microdomain structure exists in the melt. The SAXS curve at 70 °C has diffuse scattering peaks, the positions of which also correspond to a ratio of 1:2:3, suggesting the lamellar

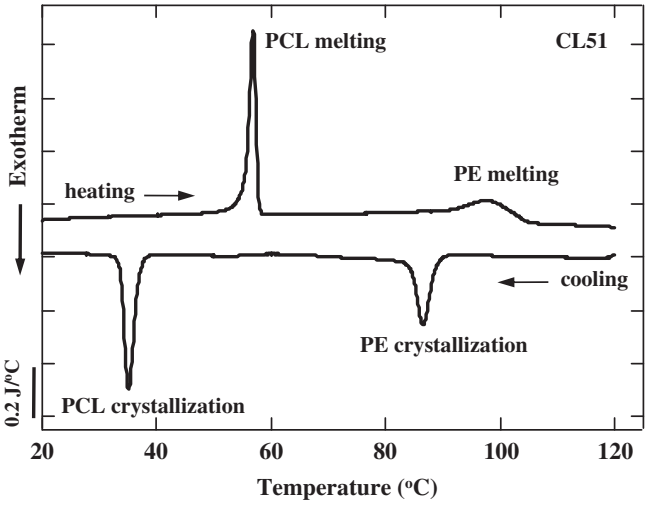

Fig. 1. DSC curves of CL51 during cooling at −5 °C/min from 120 °C (microphase-separated melt) into 0 °C and during heating at 5 °C/min from 0 °C into 120 °C. CL51 was crystallized at 0 °C for 5 min before heating.

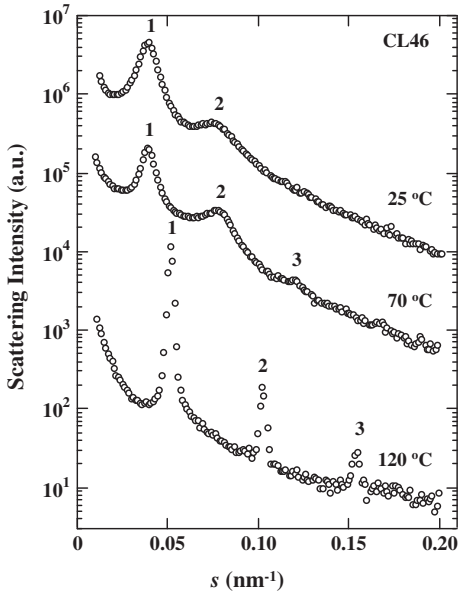

Fig. 2. 1D-SAXS curves of CL46 measured at 120 °C (bottom), 70 °C (middle), and 25 °C (top). The SAXS curves at 70 and 25 °C are successively shifted upward for legibility.

morphology is formed. However, the primary peak position is extremely different between the SAXS curves at 120 °C and 70 °C, which indicates that morphological transition has occurred from the molten lamellar microdomain into the crystallized lamellar morphology, an alternating structure consisting of crystallized PE lamellae and amorphous PCL layers (PE lamellar morphology). This transition was always observed in CL33–CL51 just after crystallization of PE blocks when they were quenched from the microphase-separated melt into low temperatures. The SAXS curve at 25 °C is not so different from that at 70 °C, in particular, the primary peak position is practically unchanged, suggesting that the PCL blocks crystallize within the PE lamellar morphology without further morphological transition. Therefore, the crystallization of PCL blocks is confined in the PE lamellar morphology. It should be noted that in our previous studies [25,26], we found a small change in the primary peak position by the crystallization of PCL blocks at $T_c \geq 35$ °C, which was ascribed to the possible distortion of the PE lamellar morphology. In this study, we mainly used lower T_c (≤30 °C), and the shift of the primary peak position could not be detected in every sample.

The uniaxial orientation of the PE lamellar morphology was carried out at 80 °C by applying the rotational shear. Fig. 3a–c shows the 2D-SAXS patterns of sheared CL51 at T_c = 70 °C (PE blocks crystallized and PCL blocks amorphous) observed from *X*, *Y*, and *Z* directions, where *X* represents the shear direction and *Y* and *Z* directions are perpendicular to the shear direction (Fig. 3, top). We find several diffraction spots on the meridian (indicated by numbers) arising from the parallel stacks of the PE lamellar morphology when viewed from *X* and *Y* directions (Fig. 3a and b), whereas no diffraction spot can be observed when viewed from *Z* direction (Fig. 3c). Fig. 3a–c clearly indicates that the PE lamellar morphology is preferentially oriented parallel to the shear direction applied to the sample, as schematically shown by the illustration. These diffraction patterns do not change so much after crystallization of PCL blocks at 25 °C (Fig. 3d–f) except the lack of third diffraction spot. That is, Fig. 3 indicates that the uniaxial orientation of the PE lamellar morphology is substantially preserved after crystallization of PCL blocks in CL51. The preservation of the uniaxially oriented PE lamellar morphology was also verified for CL33,

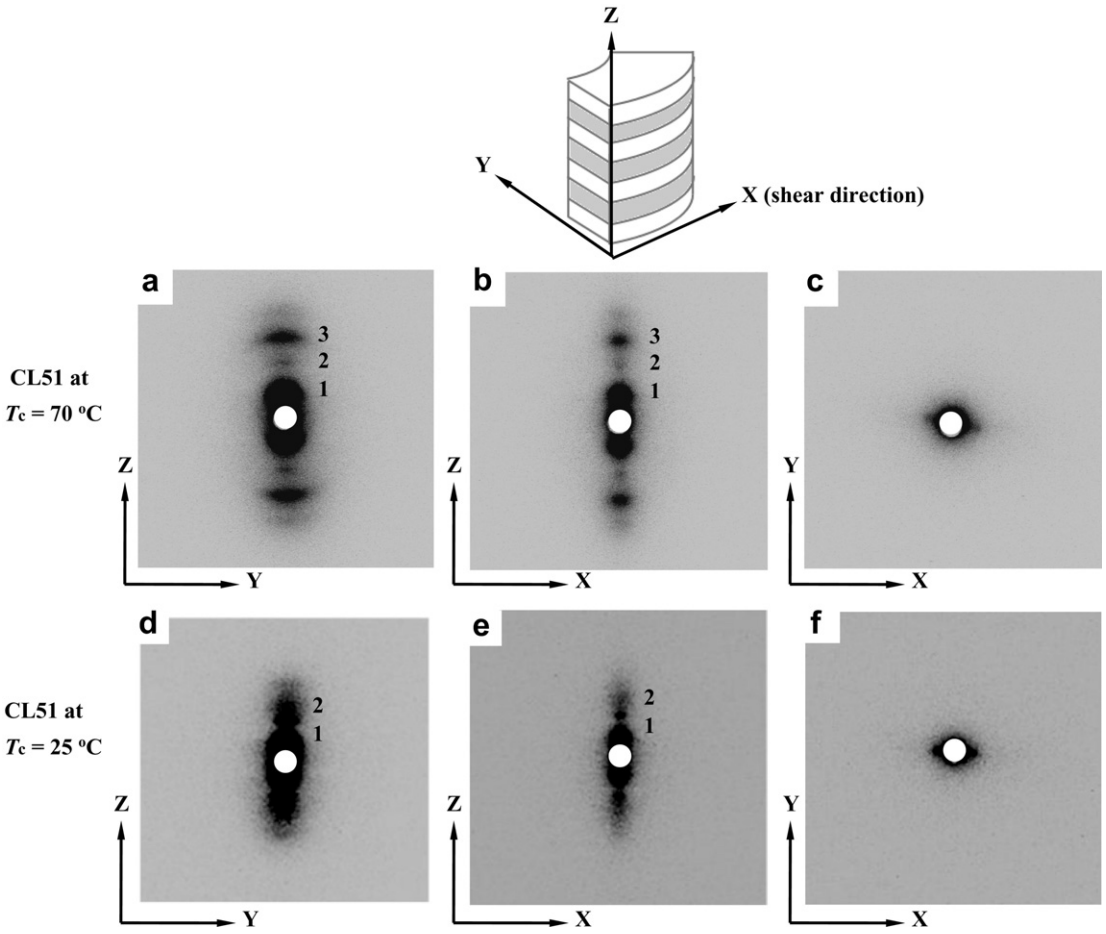

Fig. 3. 2D-SAXS patterns of uniaxially oriented CL51 at 70 °C (upper panels) and 25 °C (lower panels) when viewed from *X* (a, d), *Y* (b, e), and *Z* (c, f) directions. The definition of each direction against the shear direction is shown in the illustration (top).

CL38, and CL46 (Fig. 4). Therefore, we can investigate the crystal orientation of PCL blocks confined in the oriented PE lamellar morphology.

In summary, PCL-*b*-PE copolymers synthesized in this study formed the PE lamellar morphology after crystallization of PE blocks by destroying the molten microdomain structure, followed by PCL crystallization within the PE lamellar morphology, as revealed by 1D-SAXS results (Fig. 2). The PE lamellar morphology could be preferentially oriented parallel to the shear direction by applying the rotational shear, which was confirmed using 2D-SAXS (Figs. 3 and 4). Therefore, we can investigate the crystal orientation of PCL blocks confined in the PE lamellar morphology.

3.2. Crystal orientation of PCL blocks confined in PE lamellar morphology

The PCL blocks confined in the PE lamellar morphology were crystallized at several temperatures ranging from 0 °C to 45 °C, and orientation of PCL crystals was investigated using 2D-WAXD. Fig. 5 shows the typical WAXD patterns of CL51 before (upper panels) and after (lower panels) crystallization of PCL blocks observed from *X* (a, d), *Y* (b, e), and *Z* (c, f) directions, where the definition of each direction against the shear direction is provided in Fig. 3, top. Before crystallization of PCL blocks (T_c = 70 °C), we have clear two diffractions in every WAXD pattern, which are located at diffraction angle 2θ = 21.5° and 23.8° corresponding to the (110) and (200) diffractions from PE crystals [34], as indicated in Fig. 5a. These (110) and (200) diffractions have intensity peaks at off-axis regions when viewed from *X* and *Y* directions, suggesting that the *c* axis of PE crystals is not parallel but tilts moderately against the lamellar surface normal, for which it is reported that the shear applied to the samples in order to orient the PE lamellar morphology is responsible [35,36].

We have additional diffractions in the WAXD patterns after crystallization of PCL blocks, as shown in Fig. 5d and e. Unfortunately, the crystal structure of PE blocks is very close to that of PCL blocks [37], and therefore major diffractions from PE and PCL crystals appear at the similar diffraction angles in the WAXD pattern. However, the (110) and (200) diffractions from PCL crystals when viewed from *X* and *Y* directions give the strong intensity arcs centered on the equator, so that the combined diffraction pattern at 30 °C (d, e) is significantly different from that at 70 °C (a, b). Therefore, it is possible to evaluate the WAXD pattern only from PCL crystals by decomposing the combined diffraction pattern into two using the computational method described in the next section. When viewed from *Z* direction (c, f), on the other hand, the WAXD pattern is almost isotropic and does not change before and after crystallization of PCL blocks, though the diffraction intensities considerably increase after PCL crystallization.

The WAXD patterns of CL51 after crystallization of PCL blocks (lower panels in Fig. 5) are almost independent of T_c, but this is not the case for CL33. Fig. 6 shows the 2D-WAXD patterns of CL33 crystallized at 0 °C (a), 30 °C (b), and 45 °C (c) when viewed from *Y* direction. The WAXD pattern at 0 °C is significantly different from

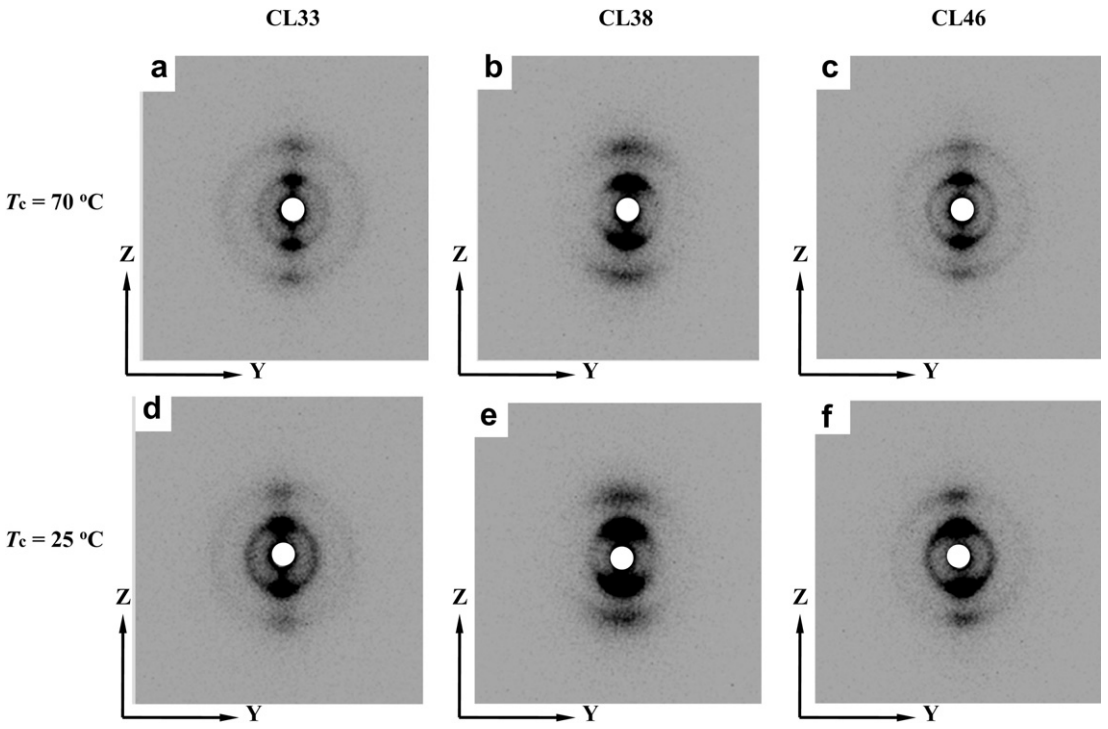

Fig. 4. 2D-SAXS patterns of uniaxially oriented CL33 (a, d), CL38 (b, e), and CL46 (c, f) at 70 °C (upper panels) and 25 °C (lower panels) when viewed from *X* direction.

that at 30 °C and 45 °C. That is, the total WAXD pattern, which arises from PE + PCL crystals, is similar to that from PE crystals (Fig. 5b), suggesting that the WAXD pattern from PCL crystals is nearly isotropic. On the other hand, the WAXD patterns at 30 and 45 °C have the strong (110) intensity around the equator as compared with that from PE crystals (Fig. 5b). Fig. 6 clearly indicates that the orientation of PCL crystals in CL33 depends significantly on T_c.

In Fig. 7, we schematically illustrate the 2D-WAXD patterns of CL51 at 70 °C (a) and 30 °C (b) when viewed from *Y* direction, where we emphasize the (110) and (200) diffractions from PE crystals by the grey arcs and those from PCL crystals by the black arcs. In addition, in order to intuitively understand the 1D-WAXD curves at 70 °C and 30 °C, the total intensity in a sector between $\phi = 73°$ and 74° is radially plotted against diffraction angle 2θ in Fig. 7c. The (110) and (200) diffraction intensities from PE crystals are

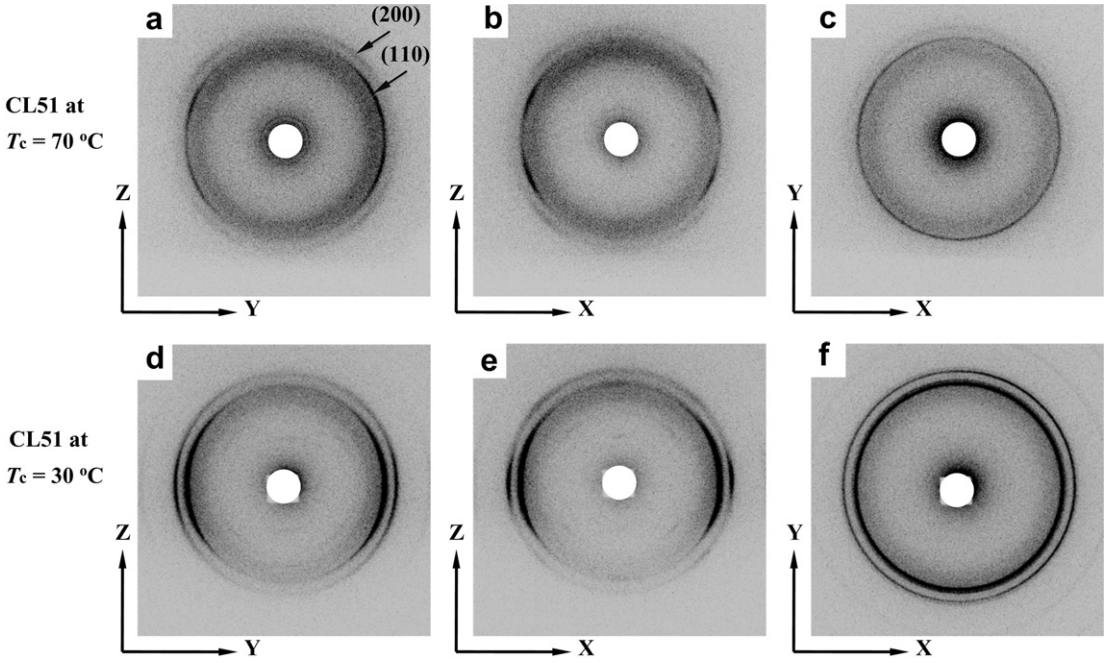

Fig. 5. 2D-WAXD patterns of CL51 at 70 °C (upper panels) and 30 °C (lower panels) when viewed from *X* (a, d), *Y* (b, e), and *Z* (c, f) directions, where only PE blocks are crystallized at 70 °C and both PE and PCL blocks are crystallized at 30 °C. The definition of each direction against the shear direction is provided in Fig. 3, top.

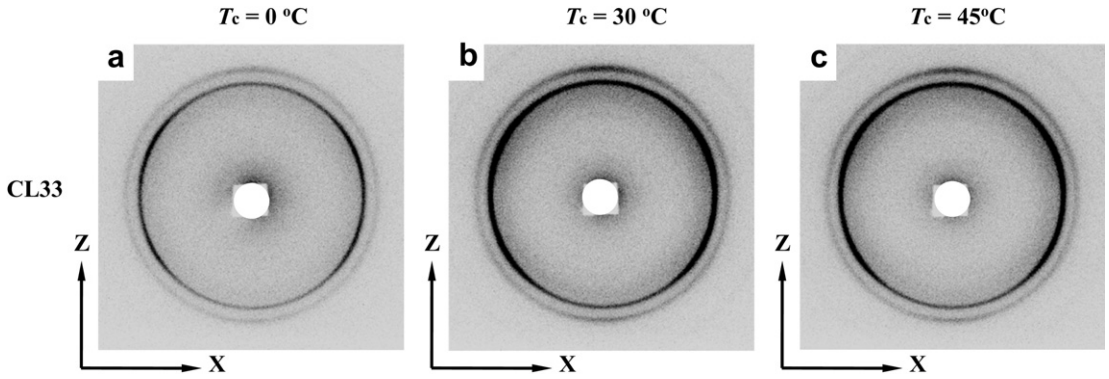

Fig. 6. 2D-WAXD patterns of CL33 crystallized at 0 °C (a), 30 °C (b), and 45 °C (c) when viewed from *Y* direction, where both PE and PCL blocks are crystallized.

significantly smaller than those from PCL crystals. Therefore it is reliable to evaluate the diffraction curve only from PCL crystals by simple subtraction using those from PE crystals (at 70 °C) and PE + PCL crystals (at 30 °C). The subtracted diffraction curve thus obtained (Fig. 7c, bottom) did not show any inconsistent results when it was plotted against the azimuthal angle, suggesting that the crystal orientation of PE blocks remains unchanged during cooling from 70 °C to 30 °C.

Fig. 8 shows the integrated intensity of the (110) diffraction from PCL crystals i.e., peak area under the (110) diffraction shown in Fig. 7c, plotted against azimuthal angle ϕ for CL33 (a) and CL51 (b) crystallized at selected temperatures indicated. In the diffraction curves of CL33 crystallized at 25 °C, 30 °C, and 45 °C, we find four distinct peaks at off-axis regions, the positions of which are almost independent of T_c. These diffraction curves with four peaks imply that the *c* axis of PCL crystals is perpendicular to the lamellar surface normal [37]. On the other hand, the (110) diffraction curve at 0 °C is almost isotropic with faint peaks at 90° and 270°, suggesting that orientation of PCL crystals is almost random except a minor component with the *c* axis being parallel to the lamellar surface normal. Therefore, we conclude that the orientation of PCL crystals formed in CL33 depends significantly on T_c. When we consider the ϕ dependence of the (110) diffraction intensities for CL51 (Fig. 8b), we find two distinct peaks at 90° and 270° at every T_c, indicating that the *c* axis of PCL crystals is parallel to the lamellar surface normal irrespective of T_c. It should be noted that the azimuthal profile of the (200) diffraction included more scattering of data points, though it was roughly consistent with the crystal orientation of PCL blocks determined from the (110) diffraction profile. The ϕ dependence of the (110) diffraction for CL38 and CL46 was similar to that of CL51 (Fig. 8b) at every T_c, though it was slightly different depending on the samples; the diffraction peaks became broader with decreasing d_{PCL}. This difference might arise from the degree of PCL crystal orientation *f* in the PE lamellar morphology, so we will evaluate *f* for each PCL-*b*-PE as a function of T_c in the next section.

In summary, the 2D-WAXD patterns of CL33 observed from *Y* (and also *X*) direction indicated that the *c* axis of PCL crystals was

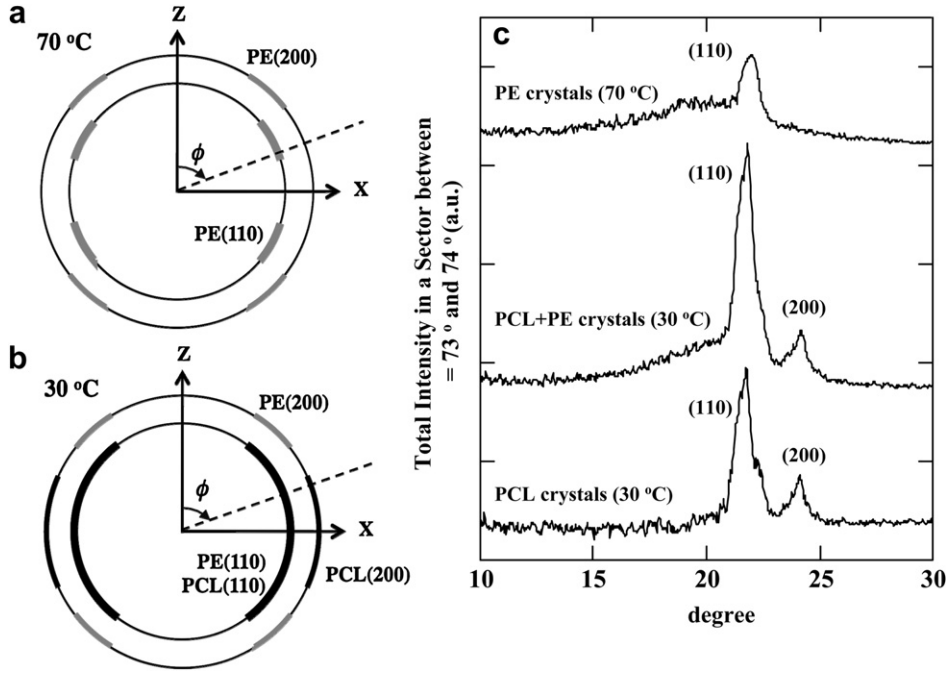

Fig. 7. (a) Schematic 2D-WAXD pattern of CL51 at 70 °C corresponding to Fig. 5b, where only PE blocks are crystallized. (b) Schematic 2D-WAXD pattern of CL51 at 30 °C corresponding to Fig. 5e, where both PE and PCL blocks are crystallized. (c) Total diffraction intensity in a sector between $\phi = 73°$ and 74° plotted against diffraction angle 2θ to intuitively show the 1D-WAXD curve from PE crystals (corresponding to a), PE + PCL crystals (b), and PCL crystals.

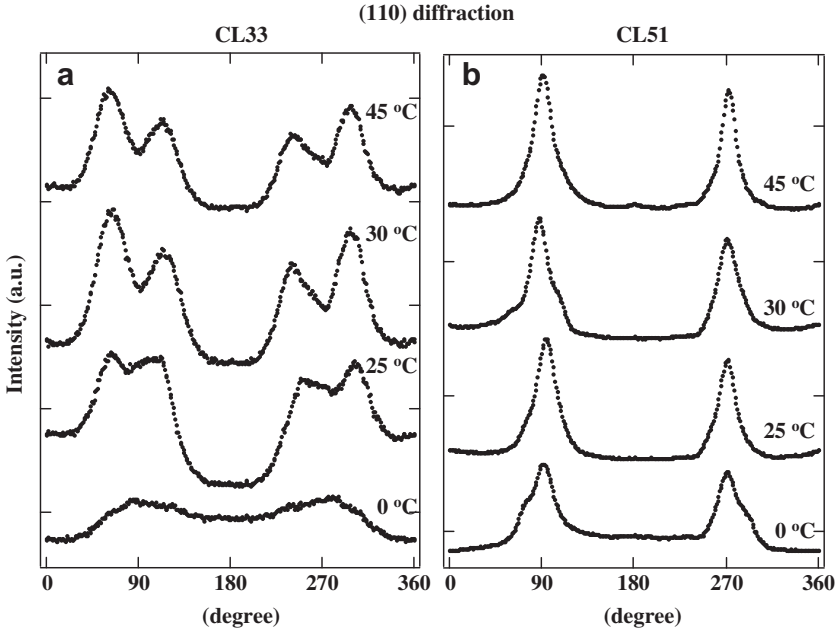

Fig. 8. The intensity of the (110) diffraction from PCL crystals plotted against azimuthal angle ϕ for CL33 (a) and CL51 (b) at selected temperatures indicated. The plots at 25 °C, 30 °C, and 45 °C are successively shifted upward for legibility.

perpendicular to the PE lamellar surface normal at 25 °C $\leq T_c \leq$ 45 °C. On the other hand, it was almost isotropic at 0 °C $\leq T_c \leq$ 20 °C except the faint diffraction peaks appearing at $\phi = 90°$ and 270°, suggesting that the crystal orientation was almost random. The 2D-WAXD patterns of CL38–CL51 crystallized at every T_c indicated that the *c* axis of PCL crystals was parallel to the PE lamellar surface normal irrespective of T_c. The small difference in the WAXD patterns among CL38–CL51 will be intimately related to the degree of PCL crystal orientation *f* in the PE lamellar morphology.

3.3. T_c and d_{PCL} dependence of PCL crystal orientation

Several methods are known to evaluate the degree of crystal orientation *f* from the ϕ dependence of 2D-WAXD patterns [38,39]. Here, we follow the same calculation procedure in our previous study [32] to evaluate *f*. That is, we evaluate *f* from the ϕ dependence of the (110) diffraction from PCL crystals using the following equation,

$$f = \frac{k^{-1} < \cos^2 \phi > -1}{k^{-1} - 1} \tag{3}$$

where *k* represents $< \cos^2 \phi >$ at random orientation (usually $k = 1/3$), and $< \cos^2 \phi >$ of the present case is calculated by,

$$< \cos^2 \phi > = \frac{\int_0^{\pi/2} I(\phi)\cos^2(\phi - \sigma)|\sin(\phi - \sigma)|\mathrm{d}\phi}{\int_0^{\pi/2} I(\phi)|\sin(\phi - \sigma)|\mathrm{d}\phi} \tag{4}$$

where $I(\phi)$ is the 1D intensity of the (110) diffraction from PCL crystals and σ is the azimuthal angle giving the maximum (110) diffraction between $\phi = 0$ and $\pi/2$ ($\sigma = \pi/2$ in Fig. 8b). Actually, we first evaluated *k* assuming $I(\phi) =$ const, then calculated *f* at each quadrant, and finally four values were averaged to evaluate *f* at each T_c for CL33–CL51. It should be noted that the four-spot diffraction pattern (Fig. 8a) was first decomposed into each diffraction peak using the Gaussian function and then Eq. (3) was applied to each quadrant. In addition, we phenomenologically evaluated *f* using the following equation [39] for the two-spot diffraction patterns (Fig. 8b),

$$f = \frac{180 - w}{180} \tag{5}$$

where *w* is the full width at half maximum (FWHM) of the diffraction peak. The T_c dependence of *f* evaluated from Eq. (5) is qualitatively similar to that obtained from Eq. (3), so we present *f* evaluated from Eq. (3) and discuss the relation between *f* and T_c (and also d_{PCL}).

Fig. 9 shows the T_c dependence of *f* for CL51 (d_{PCL} = 16.5 nm), CL46 (11.7 nm), CL38 (10.7 nm), and CL33 (8.8 nm) calculated from Eq. (3). We find that *f* for CL51–CL38 is almost constant irrespective of T_c and slightly decreases with decreasing d_{PCL}. That is, the PCL crystals in the PE lamellar morphology orient preferentially with

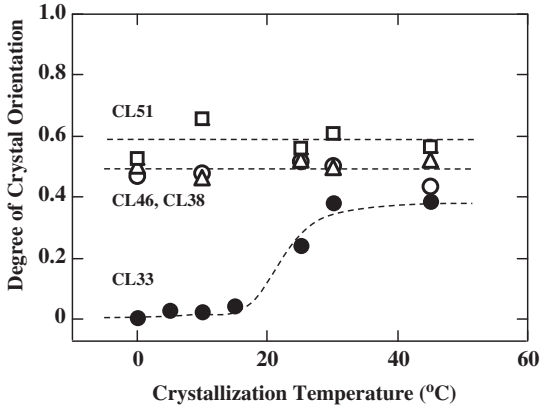

Fig. 9. Degree of PCL crystal orientation *f* plotted against crystallization temperature for CL51 (square), CL46 (triangle), CL38 (open circle), and CL33 (closed circle).

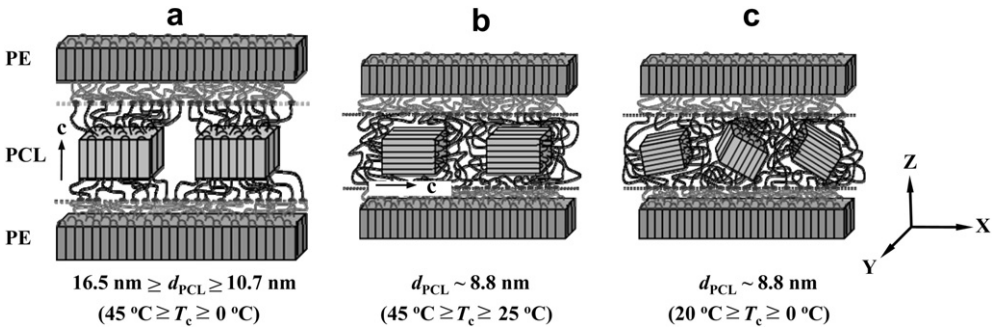

Fig. 10. Schematic illustration showing the orientation of PCL crystals spatially confined in the PE lamellar morphology at different d_{PCL} and T_c.

keeping the orientational direction at each T_c, but less oriented PCL crystals increase a little bit with decreasing d_{PCL}. This d_{PCL} dependence of f should be intimately related to the crystallization mechanism in the confined space. Fig. 9 also shows the T_c dependence of f for CL33, where we find the significant change in f with changing T_c; at 0 °C ≤ T_c ≤ 20 °C, f is almost 0, meaning the nearly random orientation of PCL crystals. However, f increases drastically at T_c ~25 °C and takes a finite value (~0.4) at 25 °C ≤ T_c ≤ 45 °C, suggesting that the preferential orientation of PCL crystals appears in the PE lamellar morphology. Because the WAXD patterns of CL33 at 45 °C ≥ T_c ≥ 25 °C shown in Fig. 8a are completely different from those of CL51 shown in Fig. 8b, it is clear that the orientation of PCL crystals in CL33 is substantially different from that in CL51. That is, we find from the crystal structure of PCL [37] that the c axis of PCL crystals is perpendicular to the PE lamellar surface normal in CL33 while it is parallel in CL51.

As a summary of this section, Fig. 10 schematically shows the orientation of PCL crystals confined in the PE lamellar morphology as a function of d_{PCL} and T_c. At 16.5 nm ≥ d_{PCL} ≥ 10.7 nm (CL38–CL51), the c axis of PCL crystals was parallel to the PE lamellar surface normal irrespective of T_c (Fig. 10a), where the degree of crystal orientation decreased slightly with decreasing d_{PCL}. At d_{PCL} = 8.8 nm (CL33), the orientation of PCL crystals depended significantly on T_c; at 45 °C ≥ T_c ≥ 25 °C the PCL crystals preferentially oriented such that the c axis was perpendicular to the PE lamellar surface normal (Fig. 10b), while the orientation was almost random at 20 °C ≥ T_c ≥ 0 °C (Fig. 10c). The crystal orientation at each T_c and d_{PCL} should be intimately related to the crystallization mechanism of PCL blocks confined in the PE lamellar morphology.

3.4. Comparison with other experimental results

Several studies have been reported on the crystallization behavior and resulting morphology of block chains confined in glassy (or hard) lamellar microdomain structures [16–23]. Cheng et al. [18–20], for example, studied crystal orientation of polyethylene oxide (PEO) blocks in the lamellar microdomain of PEO-*block*-polystyrene (PEO-*b*-PS) as a function of T_c and thickness of PEO layers d_{PEO}, and found that the c axis of PEO crystals changed with increasing T_c from random to perpendicular, then to inclined, and finally to parallel against the PS lamellar surface normal. They also reported that the initial stage of PEO crystal growth critically determined the final crystal orientation in the lamellar microdomain. Later they showed a combined effect of T_c and d_{PEO} on the crystal orientation of PEO blocks; the intermediate T_c range between perpendicular and parallel orientations was reduced with increasing d_{PEO}. Sun et al. [21,22] reported the crystal orientation of PCL blocks confined in the lamellar microdomain of PCL-*block*-poly(4-vinylpyridene) (PCL-*b*-P4VP) as a function of T_c and d_{PCL}, and obtained the consistent results with those of Cheng et al. They discussed the crystallization mechanism of block chains confined in glassy microdomains and showed that it changed from heterogeneous to homogeneous nucleation with decreasing d_{PCL}. They concluded this change in the crystallization mechanism was responsible for the difference in crystal orientation of PCL blocks with changing d_{PCL}.

Our results for the crystal orientation of PCL blocks confined in the PE lamellar morphology qualitatively agree with those of block chains confined in glassy lamellar microdomains described above. That is, we observed that the c axis of PCL crystals was parallel to the PE lamellar surface normal at 16.5 nm ≥ d_{PCL} ≥ 10.7 nm irrespective of T_c. In addition, we detected random or perpendicular orientation at d_{PCL} = 8.8 nm depending on T_c, though we could not observe parallel orientation at higher T_c. One of the possible reason was that we did not make extensive crystallization experiments at higher T_c, because the crystallization of PCL blocks might distort the existing PE lamellar morphology [25,26,29] to change the confined environment. By comparing our experimental results with those of Cheng et al. and Sun et al., we conclude that the PE lamellar morphology plays a similar role to glassy lamellar microdomains regarding spatial confinement against the crystallization of PCL blocks. This may arise from the fact that the PE lamellae in the PE lamellar morphology are hard inside and hence the deformation of these lamellae is not allowed during crystallization to show the hard nature of confined materials regarding spatial confinement.

Ho et al. investigated the crystal orientation of block chains confined in rubbery (or soft) lamellar microdomains using a poly(L-lactide)-*block*-PS (PLLA-*b*-PS) copolymer [24], where the crystallization temperature of PLLA blocks $T_{c,PLLA}$ could be intentionally controlled to be higher than the glass transition temperature of PS blocks. They found a unique undulated morphology after crystallization of PLLA blocks, where the c axis of PLLA crystals was always parallel to the PS lamellar surface normal. They concluded that this undulated morphology was originated from the heterogeneous nucleation in the confined space, as is the case for the higher T_c crystallization of block chains confined in the glassy lamellar microdomains. As a result, the c axis of PLLA crystals always oriented parallel to the PS lamellar surface normal and simultaneously the undulation of the lamellar morphology appeared due to the soft nature of confined materials for increasing the total crystallinity of PLLA blocks. These results obtained in PLLA-*b*-PS are not consistent with ours, because we observed the random and perpendicular orientation but not the parallel orientation for PCL crystallization in CL33.

In summary, the previous experimental results for the crystal orientation of block chains confined in glassy (or hard) lamellar microdomain structures qualitatively agreed with our results. It may arise from the fact that the PE lamellae in the PE lamellar morphology are hard inside and therefore the undulation of these

lamellae will not be allowed during crystallization, as is the case for the glassy PS and P4VP lamellae observed in PEO-*b*-PS and PCL-*b*-P4VP copolymers.

4. Conclusions

We have investigated the crystal orientation of poly(ε-caprolactone) (PCL) blocks, spatially confined in the solid lamellar morphology formed by the crystallization of polyethylene (PE) blocks (PE lamellar morphology) in PCL-*block*-PE copolymers, as a function of crystallization temperature T_c and confinement size d_{PCL}. The crystallizable temperature of PE blocks was sufficiently higher than that of PCL blocks, so that the PE blocks always crystallized first to form the PE lamellar morphology followed by the crystallization of PCL blocks starting from this morphology. As a result, the PE lamellar morphology worked as a kind of spatial confinement against the crystallization of PCL blocks, and it was expected to be intermediate between hard and soft confinements. The PE lamellar morphology could be uniaxially oriented using the rotational shear in order to investigate the crystal orientation of PCL blocks existing in it. The *c* axis of PCL crystals (i.e., stem direction of folded chains) was parallel to the PE lamellar surface normal irrespective of T_c when 16.5 nm $\geq d_{PCL} \geq$ 10.7 nm. However, it depended significantly on T_c when $d_{PCL} = 8.8$ nm; at 45 °C $\geq T_c \geq$ 25 °C the *c* axis was perpendicular to the lamellar surface normal while it was almost random at 20 °C $\geq T_c \geq$ 0 °C. By comparing our results with previous ones, the PE lamellar morphology was found to play a similar role to glassy lamellar microdomains (hard confinement) regarding spatial confinement against subsequent PCL crystallization.

Acknowledgment

The 1D-SAXS measurement has been performed under the approval of Photon Factory Advisory Committee (No. 2008G031).

References

[1] Hamley IW, editor. Developments in block copolymer science and technology. New York: Wiley; 2004.
[2] Muller AJ, Balsamo V, Arnal ML. Adv Polym Sci 2005;190:1–63.
[3] Nandan B, Hsu JY, Chen HL. J Macromol Sci Part C 2006;46:143–72.
[4] Castillo RV, Muller AJ. Prog Polym Sci 2009;34:516–60.
[5] Nojima S, Tanaka H, Rohadi A, Sasaki S. Polymer 1998;39:1727–34.
[6] Quiram DJ, Register RA, Marchand GR, Adamson DH. Macromolecules 1998;31:4891–8.
[7] Weimann PA, Hajduk DA, Chu C, Chaffin KA, Brodil JC, Bates FS. J Polym Sci B Polym Phys 1999;37:2053–68.
[8] Shiomi T, Tsukada H, Takeshita H, Takenaka K, Tezuka Y. Polymer 2001;42:4997–5004.
[9] Chen HL, Hsiao SC, Lin TL, Yamauchi K, Hasegawa H, Hashimoto T. Macromolecules 2001;34:671–4.
[10] Huang P, Zhu L, Cheng SZD, Ge Q, Quirk RP, Thomas EL, et al. Macromolecules 2001;34:6649–57.
[11] Loo YL, Register RA, Ryan AJ, Dee GT. Macromolecules 2001;34:8968–77.
[12] Loo YL, Register RA, Ryan AJ. Macromolecules 2002;35:2365–74.
[13] Nojima S, Toei M, Hara S, Tanimoto S, Sasaki S. Polymer 2002;43:4087–90.
[14] Balsamo V, Urdaneta N, Perez L, Carrizales P, Abetz V, Muller AJ. Eur Polym J 2004;40:1033–49.
[15] Castillo RV, Muller AJ, Lin MC, Chen HL, Jeng US, Hillmyer MA. Macromolecules 2008;41:6154–64.
[16] Cohen RE, Bellare A, Drzewinski MA. Macromolecules 1994;27:2321–3.
[17] Hamley IW, Fairclough JPA, Terrill NJ, Ryan AJ, Lipic PM, Bates FS, et al. Macromolecules 1996;29:8835–43.
[18] Zhu L, Cheng SZD, Calhoun BH, Ge Q, Quirk RP, Thomas EL, et al. J Am Chem Soc 2000;122:5957–67.
[19] Zhu L, Calhoun BH, Ge Q, Quirk RP, Cheng SZD, Thomas EL, et al. Macromolecules 2001;34:1244–51.
[20] Huang P, Zhu L, Guo Y, Ge Q, Jing AJ, Chen WY, et al. Macromolecules 2004;37:3689–98.
[21] Sun YS, Chung TM, Li YJ, Ho RM, Ko BT, Jeng US, et al. Macromolecules 2006;39:5782–8.
[22] Sun YS, Chung TM, Li YJ, Ho RM, Ko BT, Jeng US. Macromolecules 2007;40:6778–81.
[23] Hsiao MS, Zheng JX, Leng S, Horn RMV, Quirk RP, Thomas EL, et al. Macromolecules 2008;41:8114–23.
[24] Ho RM, Lin FH, Tsai CC, Lin CC, Ko BT, Hsiao BS, et al. Macromolecules 2004;37:5985–94.
[25] Nojima S, Akutsu Y, Washino A, Tanimoto S. Polymer 2004;45:7317–24.
[26] Nojima S, Akutsu Y, Akaba M, Tanimoto S. Polymer 2005;46:4060–7.
[27] Nojima S, Ito K, Ikeda H. Polymer 2007;48:3607–11.
[28] Nojima S, Kiji T, Ohguma Y. Macromolecules 2007;40:7566–72.
[29] Ikeda H, Ohguma Y, Nojima S. Polym J 2008;40:241–8.
[30] Brandrup J, Immergut EH, editors. Polymer handbook. 3rd ed. New York: Wiley; 1989.
[31] Crescenzi V, Manzini G, Calzolari G, Borri C. Eur Polym J 1972;8:449–63.
[32] Nojima S, Ohguma Y, Kadena K, Ishizone T, Iwasaki Y, Yamaguchi K. Macromolecules 2010;43:3916–23.
[33] Nojima S, Kato K, Yamamoto S, Ashida T. Macromolecules 1992;25:2237–42.
[34] Swan PR. J Polym Sci 1962;56:409–16.
[35] Cui L, Miao J, Zhu L, Sics I, Hsiao BS. Macromolecules 2005;38:3386–94.
[36] Miao J, Cui L, Lau HP, Mather PT, Zhu L. Macromolecules 2007;40:5460–70.
[37] Chatani Y, Okita Y, Tadokoro H, Yamashita Y. Polym J 1970;1:555–62.
[38] Somani RH, Yang L, Hsiao BS, Sun T, Pogodina NV, Lustiger A. Macromolecules 2005;38:1244–55.
[39] Miyazaki T, Hoshiko A, Akasaka M, Sakai M, Takeda Y, Sakurai S. Macromolecules 2007;40:8277–84.